Electronic supplementary information

Spiro[fluorene-9,9'-xanthene]-based hole transporting materials for efficient perovskite solar cells with enhanced stability

Kuan Liu,[ab] Yuehan Yao,[a] Jiayu Wang,[a] Lifeng Zhu,[b] Mingli Sun,[c] Baoyi Ren,[d] Linghai Xie,[c] Yanhong Luo,[b] Qingbo Meng*[b] and Xiaowei Zhan*[a]

[a] *Department of Materials Science and Engineering, College of Engineering, Key Laboratory of Polymer Chemistry and Physics of Ministry of Education, Peking University, Beijing 100871, China. E-mail: xwzhan@pku.edu.cn*

[b] *CAS Key Laboratory for Renewable Energy, Beijing Key Laboratory for New Energy Materials and Devices, Institute of Physics, Chinese Academy of Sciences, Beijing 100190, China. E-mail: qbmeng@iphy.ac.cn*

[c] *Key Laboratory for Organic Electronics and Information Displays & Institute of Advanced Materials, National Synergistic Innovation Center for Advanced Materials, Nanjing University of Posts & Telecommunications, Nanjing, Jiangsu 210023, China*

[d] *College of Applied Chemistry, Shenyang University of Chemical Technology, Shenyang, Liaoning 110142, China*

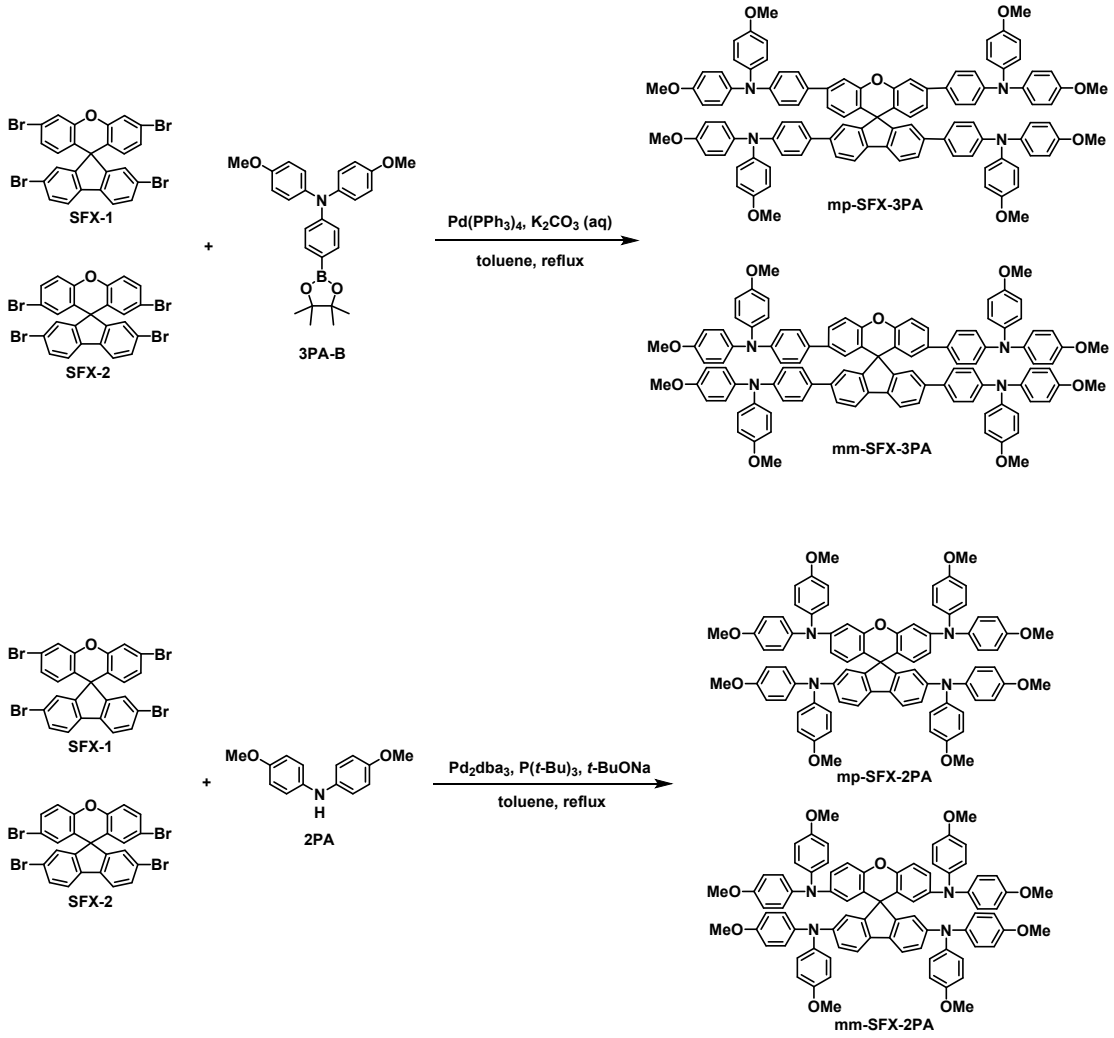

Scheme S1. Synthesis routes of four HTMs.

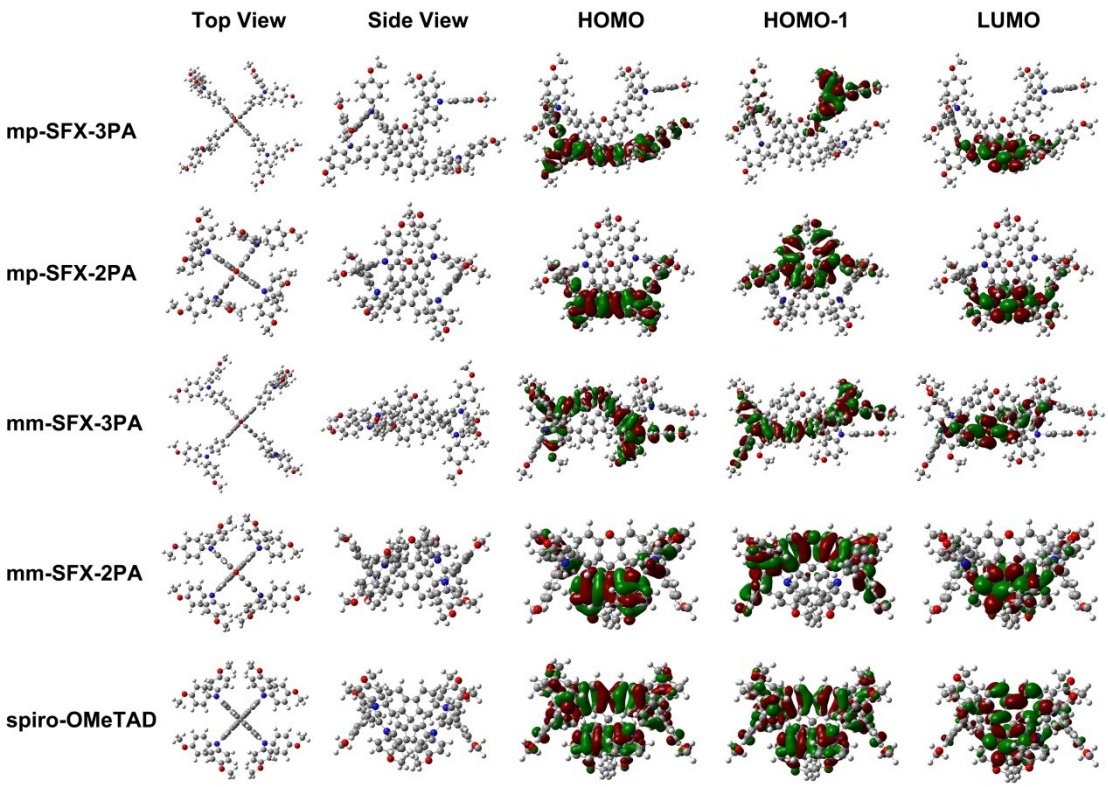

Fig S1. The optimized geometries, electron distribution of HOMO, HOMO-1 and LUMO of different HTMs.

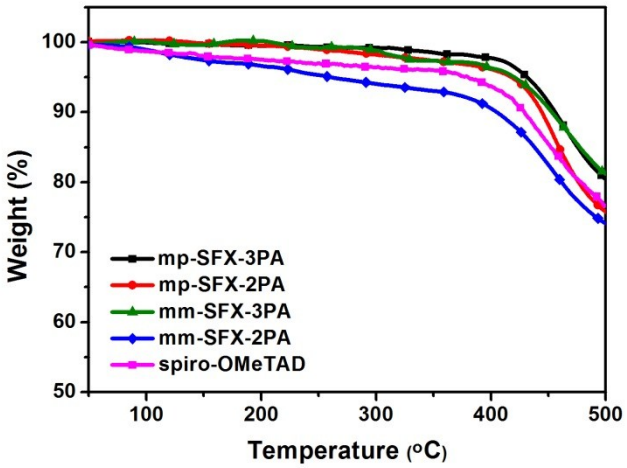

Fig S2. TGA curves of different HTMs.

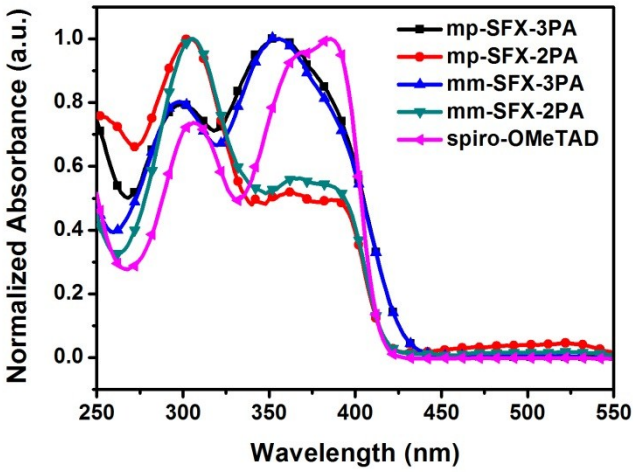

Fig S3. Normalized UV-vis absorption spectra of different HTMs in DCM solution.

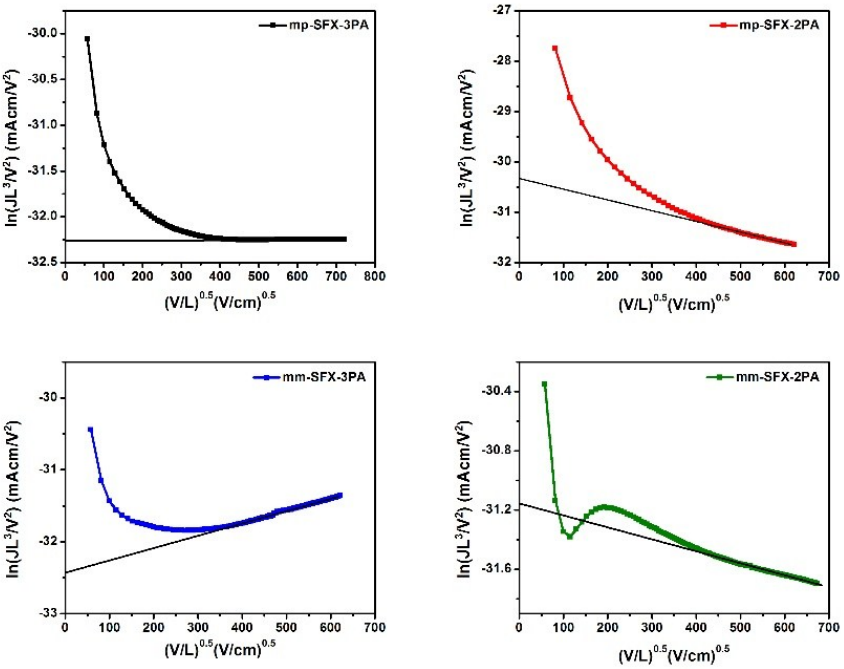

Fig S4. *J-V* characteristics of hole-only devices based on doped HTMs under dark.

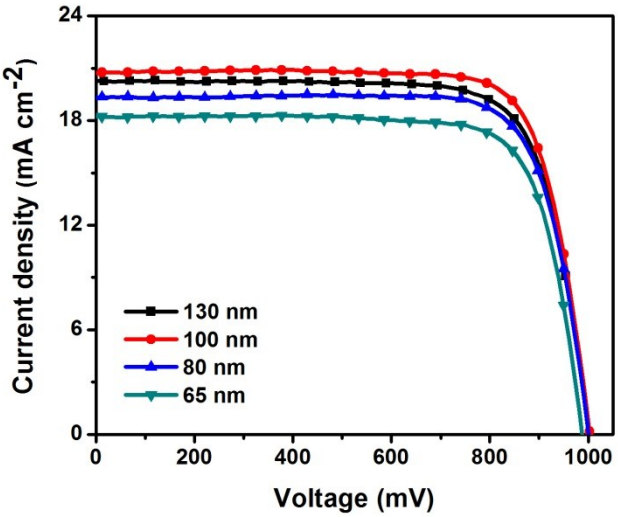

Fig S5. Effect of doped mp-SFX-2PA thickness on the performance of MAPbI3 based PSCs.

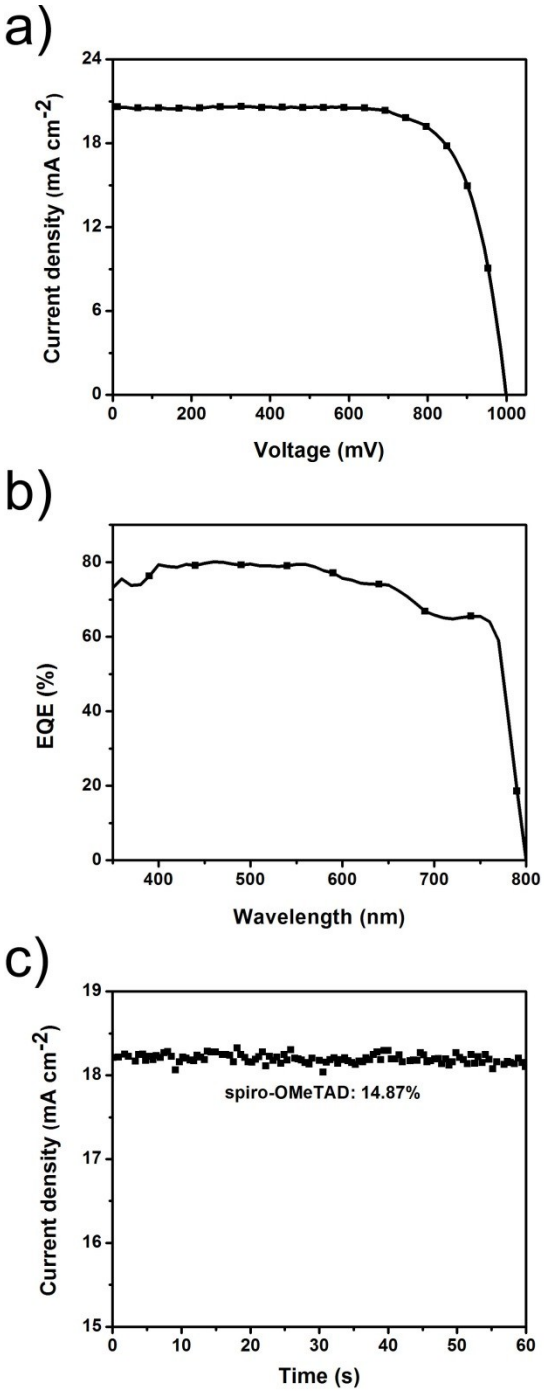

Fig S6. (a) *J-V* curve of PSC based on doped spiro-OMeTAD, measured under AM 1.5G illumination, 100 mW cm^{-2}. (b) EQE spectrum as a function of the wavelength of monochromatic light. (c) Steady-state current density and power output measured at the maximum power point (817 mV).

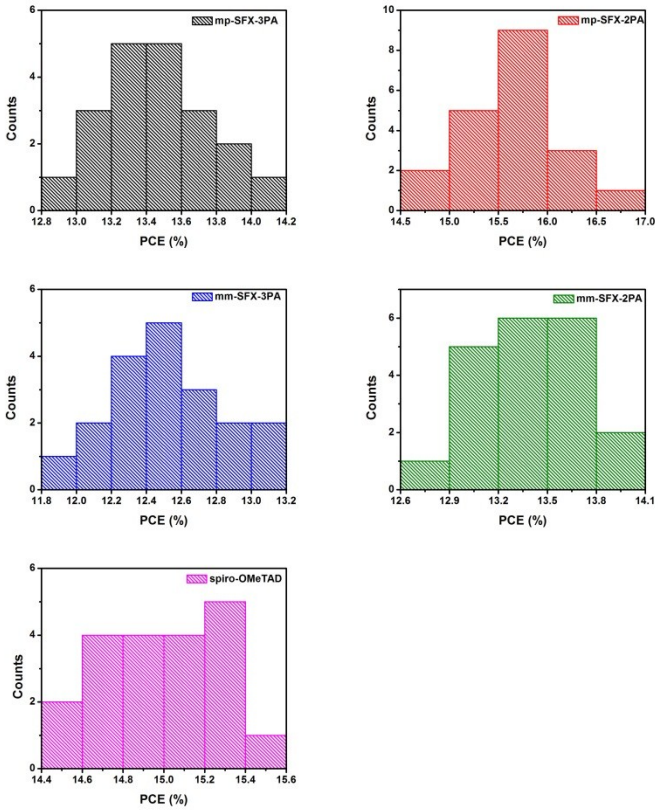

Fig S7. Statistical distribution histogram of PCEs of $MAPbI_3$ PSCs with dopant (20 devices for each case).

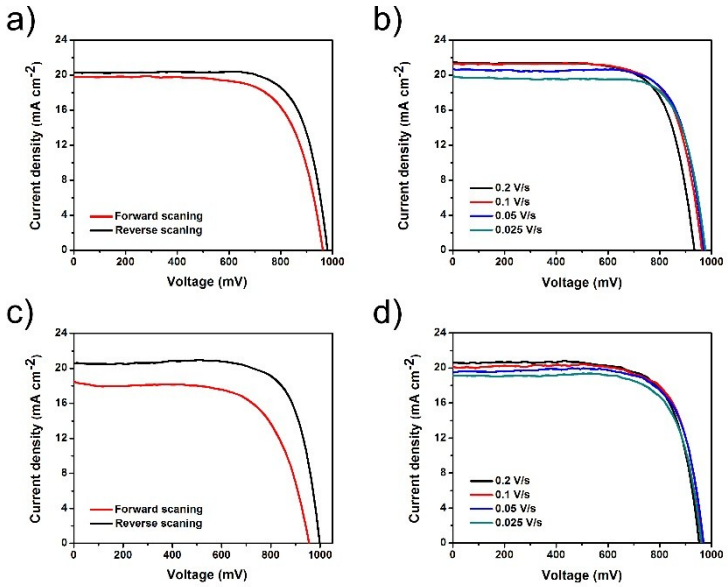

Fig S8. *J-V* curves of $MAPbI_3$ based devices with doped mp-SFX-2PA: (a) under different scanning

directions with 0.1 V/s rate, (b) under different scanning rate of reverse scanning. *J-V* curves of doped spiro-OMeTAD based devices: (c) under different scanning directions with 0.1 V/s rate, (d) under different scanning rate of reverse scanning.

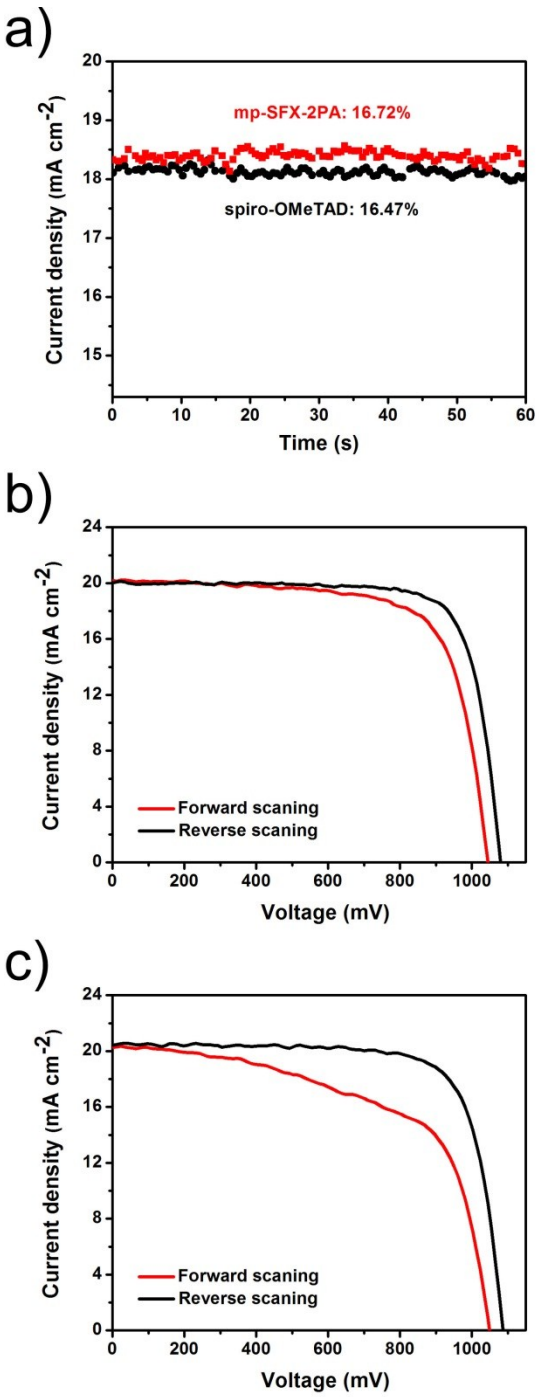

Fig S9. (a) Steady-state current density and power output for the $(FAPbI_3)_{0.85}(MAPbBr_3)_{0.15}$ based PSCs using doped mp-SFX-2PA and doped spiro-OMeTAD measured at the maximum power point.

J-V curves of the $(FAPbI_3)_{0.85}(MAPbBr_3)_{0.15}$ based PSCs employing (b) doped mp-SFX-2PA and (c) doped spiro-OMeTAD under different scanning directions with 0.1 V/s rate.

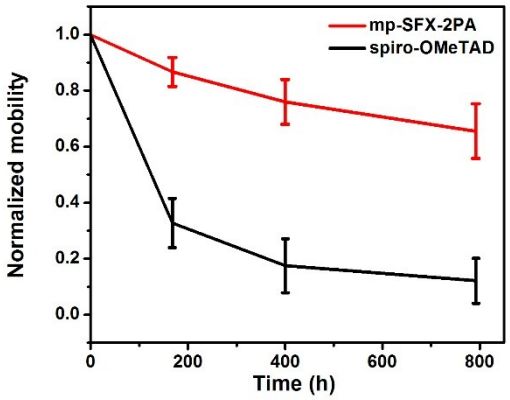

Fig S10. Normalized hole mobility as a function of time for the $MAPbI_3$ devices based on doped mp-SFX-2PA and doped spiro-OMeTAD, stored under ambient condition (20 ± 5 ^oC, 15 ± 5 % relative humidity).

Table S1. Calculated LUMO+1, LUMO, HOMO and HOMO-1 energy levels

	mp-SFX-3PA	mm-SFX-3PA	mp-SFX-2PA	mm-SFX-2PA	spiro-OMeTAD
LUMO+1	-0.67	-0.66	-0.36	-0.44	-0.65
LUMO	-1.08	-1.10	-0.65	-0.72	-0.67
HOMO	-4.47	-4.47	-4.27	-4.32	-4.27
HOMO-1	-4.57	-4.48	-4.58	-4.37	-4.29

Table S2. Photovoltaic parameters of the $MAPbI_3$ based PSCs with different thickness of doped mp-SFX-2PA

Thickness of mp-SFX-2PA (nm)	J_{SC} (mA cm^{-2})	V_{OC} (mV)	FF (%)	PCE (%)
130	20.24	1001	75.90	15.38
100	20.75	1008	77.53	16.22
80	19.33	997.0	78.00	15.03
65	18.23	986.0	77.12	13.86